Single Transformer, MMC based MV Power Electronic Traction Transformer

Simon Fuchs, Simon Beck, Jürgen Biela
Laboratory for High Power Electronic Systems (HPE)
ETH Zürich, Switzerland
Email: becksi@ethz.ch, jbiela@ethz.ch

Keywords

≪Solid-State Transformers≫, ≪Modular Multilevel Converters (MMC)≫, ≪Traction Application≫

Abstract

To reduce the number of modules and the number of transformers of existing power electronic traction transformers (PETTs), a novel PETT topology based on the principle of the modular multilevel converter (MMC) and the dual active bridge (DAB) is introduced. The paper explains the operation principle of the proposed PETT and compares the PETT to two existing concepts.

1 Introduction

Distributed traction drives in modern passenger train concepts benefit from low volume and weight alternatives to classical concepts requiring a transformer operating at grid frequency ($16\,^2/_3$ or 50 Hz). Such a transformer is inherently large in volume and often has a relatively efficiency, especially at partial loading of the traction system. In contrast, medium frequency transformers (MFT) can be designed to achieve a much lower volume with even higher efficiencies [1, 2]. However, a power electronic converter is required to generate the medium frequency AC input voltage for any MFT. In the following, such a combination of one or more MFT with a power electronic converter is called power electronic traction transformer (PETT) [3, 4].

The grid voltages in the railway power system are typically in the range of 15-25 kV, such that multilevel converters are required on the grid side of the PETT. A promising candidate to realize such a multilevel converter is the concept of the modular multilevel converter (MMC). MMCs are based on modules which are typically implementing an H-bridge in case of bidirectional/AC voltage output. Each of these modules has its own DC-link capacitor and the modules are connected in series to compose a so called MMC arm. Because malfunctioning modules can simply be bypassed during operation, the MMC also offers a high availability, because the $(n-1)$ principle can be applied without extensively over-dimensioning the converter [5, 6].

In literature, there are two main concepts for PETTs based on MMCs [7]:

- In [8], an MMC with four arms is used to feed the primary side of an MFT. The secondary side is used to supply a traditional traction drive inverter. The four arm structure results in a rather high control effort (relatively complicated modulation, energy balancing control, etc.), which is generally not beneficial.
- With the concept presented in [3, 4], only a single MMC arm connected between the line and ground is required. The module capacitor of each of the MMC modules is used as a DC link of an isolated LLC resonant DC/DC converter. The outputs of the LLC resonant converters are connected in parallel to feed a traditional traction drive inverter. This means, that there is one resonant

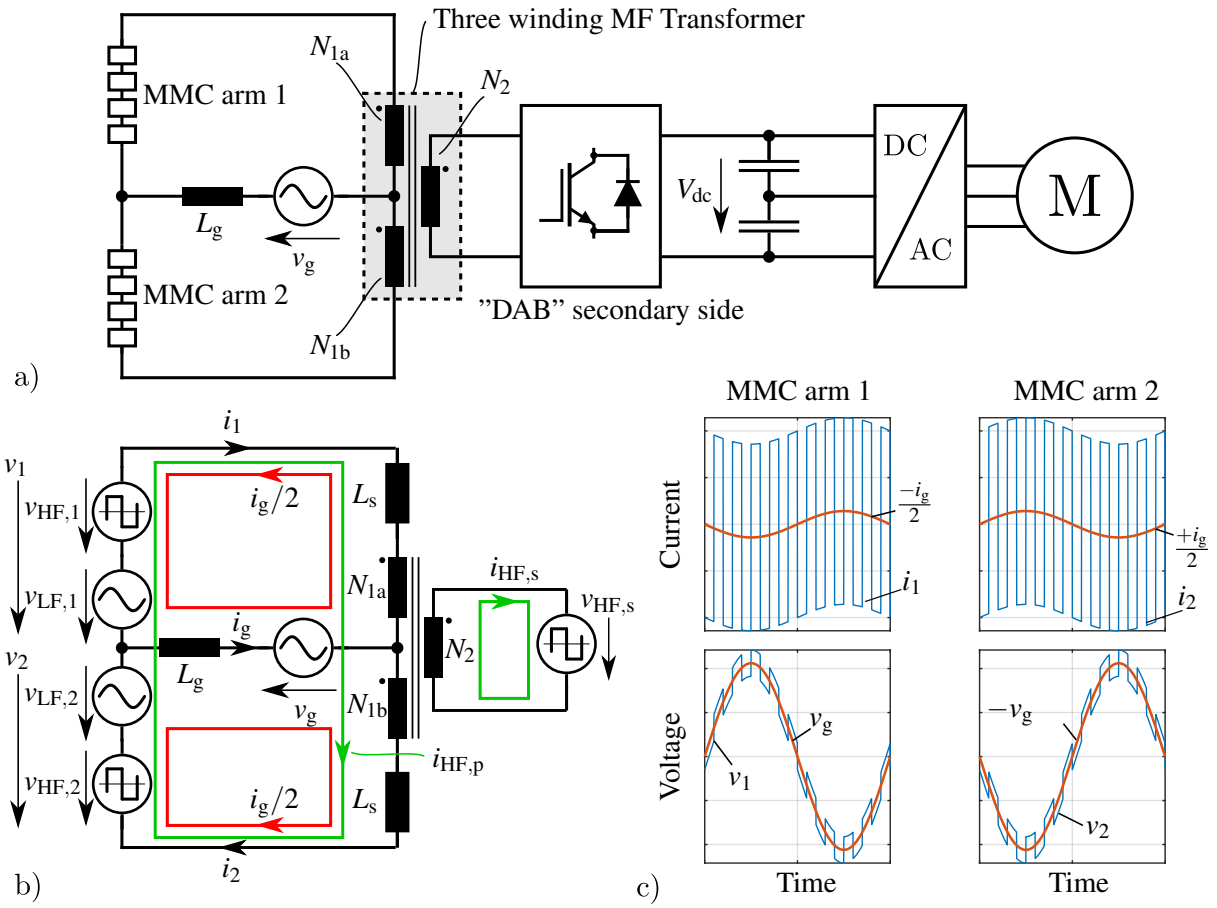

Fig. 1: a) Basic layout of the proposed PETT topology. b) Equivalent circuit of the PETT with the used currents and voltages. c) Basic waveforms for the proposed PETT if the amplitude of $i_{HF,p}$ is larger than half the grid current amplitude.

converter (including an MFT) for each MMC module. Therefore, the isolation requirements have to be fulfilled for every single module/MFT, which can result in a comparably high volume per module. On the one hand, this enables to use standard control and design schemes for the resonant converters in each module. On the other hand, it also significantly increases the system complexity, if high line voltages and therefore a high number of modules are considered.

In this paper, a concept for a PETT based on the MMC concept as shown in [8] is presented. In the presented concept, an MMC structure is used to control the grid current and to generate the primary voltage for a single three winding MFT operated as a dual-active bridge (DAB). However, only two MMC arms (instead of four in the concept from [8]) are required for the proposed concept, such that the number of required modules is lower as will be shown in the paper. Moreover, the converter can be operated in such a way, that ZVS soft-switching is always achieved. This potentially increases the efficiency compared to [3, 4], where soft-switching can only be achieved in the LLC resonant converters, while the MMC front-end operates with hard-switching.

The paper is structured as follows: First, the basic structure and operation principles of the proposed PETT are introduced and verified with simulation results. Thereafter, equations for the installed semiconductor power as well as the required energy storage in the module capacitance are derived. Finally, the proposed concept is compared with the PETT concepts presented in [3, 4] and [8].

2 Basic Converter Structure and Operation Principle

The proposed MMC based PETT consists of two MMC arms with N H-bridge modules, a medium frequency transformer (MFT) with three windings (N_{1a}, N_{1b} and N_2) as well as a full-bridge operating at

the DC-link voltage of the drive inverter connected to the third winding of the MFT as shown in Fig. 1a. The MMC arms are used to implement two voltages as shown in Fig. 1b: First, a low frequency voltage v_{LF} to compensate the grid voltage with the output voltage of each of the MMC arms and control the grid current. Second, each of the two MMC arms additionally implements the primary side of a classical dual-active bridge converter (DAB) with one or more modules providing a high frequency voltage v_{HF} to the windings $N_{1\mathrm{a}}$ and $N_{1\mathrm{b}}$ of the MFT. The secondary side of the DAB is realised with a full-bridge connected to winding N_2 of the MFT (Fig. 1b).
Basic waveforms for the proposed topology are shown in Fig. 1c). In the considered design, the amplitude of the HF part of the MMC arm currents i_1 and i_2 is larger than the amplitude of their low frequency component that corresponds to half of the grid current. Therefore, soft-switching can be achieved in all modules.
The voltage across the windings $N_{1\mathrm{a}}$ and $N_{1\mathrm{b}}$ must be synchronous without a phase-shift, such that $v_{\mathrm{HF},1} = v_{\mathrm{HF},2}$ is required. This avoids a power flow from $N_{1\mathrm{a}}$ to $N_{1\mathrm{b}}$ or vice versa.
Note that the windings $N_{1\mathrm{a}}$ and $N_{1\mathrm{b}}$ of the MFT also conduct half of the grid current i_{g} (Fig. 1c). However, because the generated magnetomotive force (MMF) $N_{1\mathrm{a}} \cdot i_{\mathrm{g}}$ is negative and $N_{1\mathrm{b}} \cdot i_{\mathrm{g}}$ is positive, the grid current i_{g} does not generate a magnetic flux in the transformer core and also no power transfer to the secondary winding N_2.

In the following, the equations for the MMC arm currents and voltages as well as the currents and voltages of the secondary side as defined in Fig. 1b) are derived. The DAB is operated with 50 % duty cycle, such that the power flow control is done via the phase shift φ_{HF} between the primary voltage $v_{\mathrm{HF},1/2}$ and the secondary voltage V_{dc} of the MFT [9].

2.1 Converter Voltages

The output voltages of MMC arm 1 and 2 are composed of the low frequency grid voltage oscillating with ω_{g} plus the high frequency rectangular transformer voltage toggling with f_{HF} for the DAB as shown in Fig. 1b:

$$v_1 = \underbrace{-V_{\mathrm{g}} \cdot \sin(\omega_{\mathrm{g}} t)}_{v_{\mathrm{LF},1}} + \underbrace{V_{\mathrm{HF}} \cdot \mathrm{rect}(f_{\mathrm{HF}} \cdot t)}_{v_{\mathrm{HF},1}}, \qquad v_2 = \underbrace{+V_{\mathrm{g}} \cdot \sin(\omega_{\mathrm{g}} t)}_{v_{\mathrm{LF},2}} + \underbrace{V_{\mathrm{HF}} \cdot \mathrm{rect}(f_{\mathrm{HF}} \cdot t)}_{v_{\mathrm{HF},2}}, \tag{1}$$

$$\text{where} \quad \mathrm{rect}(f_{\mathrm{HF}} \cdot t) = \begin{cases} +1 & \text{if } (f_{\mathrm{HF}} \cdot t \bmod 1.0) \in [0, 0.5[\\ -1 & \text{if } (f_{\mathrm{HF}} \cdot t \bmod 1.0) \in [0.5, 1.0[\end{cases} \quad \text{with 50 \% duty cycle.}$$

v_1 and v_2 are plotted in the lower part of Fig. 1c. For a given secondary side voltage amplitude V_{dc} and a specific transformer turns ration n, the amplitudes of the HF part of the MMC arms' voltages are $V_{\mathrm{HF}} = n \cdot V_{\mathrm{dc}}$. The secondary side voltage $v_{\mathrm{HF,s}}$ is expressed as

$$v_{\mathrm{HF,s}} = V_{\mathrm{dc}} \cdot \mathrm{rect}(f_{\mathrm{HF}} \cdot t - \varphi_{\mathrm{HF}}), \tag{2}$$

where φ_{HF} is the phase shift to control the power flow as shown in Fig. 2.

2.2 Converter Currents

The MMC arm currents are also composed of a low frequency grid current component and a high frequency DAB component (cf. Fig. 1b):

$$i_1 = -i_{\mathrm{LF}} + i_{\mathrm{HF,p}}, \qquad i_2 = +i_{\mathrm{LF}} + i_{\mathrm{HF,p}}, \tag{3}$$

where $i_{\mathrm{LF}} = {}^{i_{\mathrm{g}}}/_2 = {}^{P}/_{V_{\mathrm{g}}} \cdot \sin(\omega_{\mathrm{g}} t)$ with the transferred real power P.
The waveform of HF part of the current in general strongly varies with the type of the chosen modulation of the DAB [10, 11, 12]. However, assuming that the DAB is operated with 50 % duty cycle and that the ratio of the applied rectangular voltages $V_{\mathrm{HF,p}}/V_{\mathrm{dc}}$ are close to the transformer turns ratio n, the DAB transformer currents have a trapezoidal shape as shown in Fig. 2. A phase shift φ_{HF} is applied between

the two primary voltages and the secondary side voltage in order to control the power transfer

$$P_{\mathrm{HF}} = \frac{n^2 \cdot V_{\mathrm{dc}} \cdot \varphi_{\mathrm{HF}} \cdot (\pi - |\varphi_{\mathrm{HF}}|)}{\pi \cdot f_{\mathrm{HF}} \cdot L_{\mathrm{s}}}. \tag{4}$$

At rated power P_{r}, this phase shift is commonly chosen to be lower than its absolute maximum $\pi/2$ - e.g. around $\varphi_{\mathrm{HF,r}} = \pi/4$. Note that with (4) the choice of $\varphi_{\mathrm{HF,r}}$ also defines the required series inductance

$$L_{\mathrm{s}} = \frac{n^2 V_{\mathrm{dc}}^2 \cdot \varphi_{\mathrm{HF}} \cdot (\pi - \varphi_{\mathrm{HF}})}{2 P_{\mathrm{r}} \pi^2 f_{\mathrm{HF}}} = \frac{3 n^2 V_{\mathrm{dc}}^2}{16 P_{\mathrm{r}} f_{\mathrm{HF}}}. \tag{5}$$

This series inductance includes the transformer leakage inductance plus an optional dedicated inductor. The phase shift also defines the time interval $\varphi_{\mathrm{HF}}/2\pi f_{\mathrm{HF}}$ where the primary and secondary voltages are in opposite directions, such that the voltage $2nV_{\mathrm{dc}}$ is applied across the inductance L_{s} (cf. Fig. 2). The primary side HF current amplitude therefore compiles to

$$I_{\mathrm{HF,p}} = \frac{\varphi_{\mathrm{HF}}}{2\pi f_{\mathrm{HF}}} \cdot \frac{n V_{\mathrm{dc}}}{L_{\mathrm{s}}} = \frac{8 P_{\mathrm{r}}}{3 n V_{\mathrm{dc}}} \cdot \frac{\varphi_{\mathrm{HF}}}{\pi}. \tag{6}$$

At rated power with $\varphi = \pi/4$ this results in $I_{\mathrm{HF,p}} = 2P_{\mathrm{r}}/3nV_{\mathrm{dc}}$. The amplitude of the secondary current $i_{\mathrm{HF,s}}$ is given with $I_{\mathrm{HF,s}} = 2n \cdot I_{\mathrm{HF,p}}$ due to the two primary windings.

2.3 Transformer turns ratio

The transformer turns ratio $n = N_{1\mathrm{a}}/N_2 = N_{1\mathrm{b}}/N_2$ has a big impact on the operation and the design of the proposed converter: For low turns ratios, the amplitude of the HF part $I_{\mathrm{HF,p}}$ of the current in the MMC arms is relatively high. This results in a zero crossing of the currents in the MMC arms which can be used to achieve zero-voltage-switching in the MMC arms to significantly reduce the switching losses especially if SiC MOSFETs are used to implement the MMC modules.
To obtain this current zero crossing, the primary side HF current amplitude $I_{\mathrm{HF,p}}$ must be higher than the low frequency current amplitude $I_{\mathrm{g}}/2$:

$$k \cdot I_{\mathrm{HF,p}} = k \cdot \frac{2P}{3nV_{\mathrm{dc}}} > \frac{I_{\mathrm{g}}}{2} = \frac{P}{V_{\mathrm{g}}} \qquad \Leftrightarrow \qquad n_{\mathrm{ZVS}} < k \cdot \frac{2V_{\mathrm{g}}}{3V_{\mathrm{dc}}} \tag{7}$$

Here, $k < 1$ is a safety factor to ensure enough current though L_{s} to safely fulfil the ZVS conditions [13]. Note that this is only true at rated power, because the phase shift φ_{HF} and therefore also the current amplitude does not scale linearly with the transmitted power P. Therefore, to achieve ZVS also at lower power outputs, e.g. the switching frequency [10] or the modulation scheme [11, 12] can be adopted.

2.4 Semiconductor Requirements

As explained before, both MMC arms must allow a bidirectional output voltage. Therefore, only full-bridge modules are feasible. The required number of modules N depends on the module voltage V_{m} and can be calculated based on the maximum arm voltage (1) to

$$N = 2 \cdot \lceil (V_{\mathrm{g}} + n \cdot V_{\mathrm{dc}})/V_{\mathrm{m}} \rceil \tag{8}$$

including both MMC arms which results in the factor of two. The total number of switches is $4N + 4$, if full-bridge modules are assumed including the secondary side converter.

The installed semiconductor power for the MMC arms P_{sc} results from the number of modules N, the module voltage V_{m} and the maximum MMC arm current:

$$P_{\mathrm{sc,p}} = 4N \cdot V_{\mathrm{m}} \cdot (I_{\mathrm{HF,p}} + P/V_{\mathrm{g}}). \tag{9}$$

The full-bridge on the secondary side requires four switches operating at V_{dc} with a maximum current

Table I: PETT parameters

Variable	Parameter	Value(s)
P	Transmitted power	3 MW
V_g	Grid voltage	$\sqrt{2}\cdot 15\,\mathrm{kV}$
V_dc	Secondary side voltage of the transformer(s)	3 kV
V_m	Rated module voltage	$1\ldots 5\,\mathrm{kV}$
n	Transformer turns ratio	$0.95\cdot 2\,V_\mathrm{g}/3V_\mathrm{dc}$
L_s	Series inductance	2.8 mH
β	Steinmetz core loss parameter	2.5

given by $2n\cdot I_\mathrm{HF,p}$ in (6). This results in in

$$P_\mathrm{sc,s} = 4\cdot V_\mathrm{dc}\cdot 2n\cdot I_\mathrm{HF,p} = 4\cdot\frac{4P}{3}. \tag{10}$$

2.5 Required Energy Storage (Module Capacitors)

Because the proposed PETT topology basically implements a single phase AC to DC converter, the pulsating power from the single phase grid must be intermediately stored by the converter to allow a constant DC power output. Therefore, the MMC arms require a certain module capacitance value in order to provide an energy buffer. Here, the power drawn by the DAB converter on the secondary side can be assumed to be a DC power, because the operating frequency is typically two orders of magnitude higher than the AC grid frequency. The instantaneous energy fluctuation $e(t)$ of one of the MMC arms can be calculated as follows:

$$e_\mathrm{arm}(t) = \int_0^t P_\mathrm{LF}(t) - P_\mathrm{HF}dt = \int_0^t \frac{V_\mathrm{g}\cdot I_\mathrm{g}}{2}\sin^2(\omega_\mathrm{g}t) - \frac{P}{2}dt = \int_0^t P\sin^2(\omega_\mathrm{g}t) - \frac{P}{2}dt \tag{11}$$

$$= -\frac{P}{4\omega_\mathrm{g}}\sin(2\omega_\mathrm{g}t) \tag{12}$$

The peak-to-peak value of the instantaneous energy fluctuation $e_\mathrm{arm}(t)$ defines energy variation $\Delta e_\mathrm{arm} = P/2\omega_\mathrm{g}$ of the MMC arms. This peak-to-peak energy variation can be used to derive the required module capacitance value C_m with

$$\frac{\Delta e_\mathrm{arm}}{N} \leq \frac{1}{2}C_\mathrm{m}(V_\mathrm{m}+\Delta v_\mathrm{m})^2 - \frac{1}{2}C_\mathrm{m}(V_\mathrm{m}-\Delta v_\mathrm{m})^2 \quad\Leftrightarrow\quad C_\mathrm{m} \geq \frac{\Delta e_\mathrm{arm}}{2N\cdot V_\mathrm{m}\cdot\Delta v_\mathrm{m}} = \frac{P}{4N\cdot\omega_\mathrm{g}\cdot V_\mathrm{m}\cdot\Delta v_\mathrm{m}}, \tag{13}$$

where Δv_m is the allowed module voltage deviation from the rated module voltage V_m. The total required average energy storage E_cap is therefore

$$E_\mathrm{cap} = N\cdot C_\mathrm{m}\cdot V_\mathrm{m}^2 = \frac{V_\mathrm{m}\cdot P}{4\cdot\omega_\mathrm{g}\cdot\Delta v_\mathrm{m}} \tag{14}$$

for all $2N$ modules of the converter. Note that for MMCs, more sophisticated methods to derive the minimum required module capacitance exist and the operation of the MMC has great impact on the required capacitance value [14, 15, 16]. However, the complexity of the control and modulation of the DAB part would strongly increase with a high module voltage fluctuation, such that this topic exceeds the scope of this paper.

2.6 Simulation results

Figure 2 displays simulation results for the proposed PETT concept. Table I contains the associated parameters used for the simulation model. The simulation is based on average models for the MMC arms as introduced in [17], such that the current ripple in the grid current is not present. It can be seen,

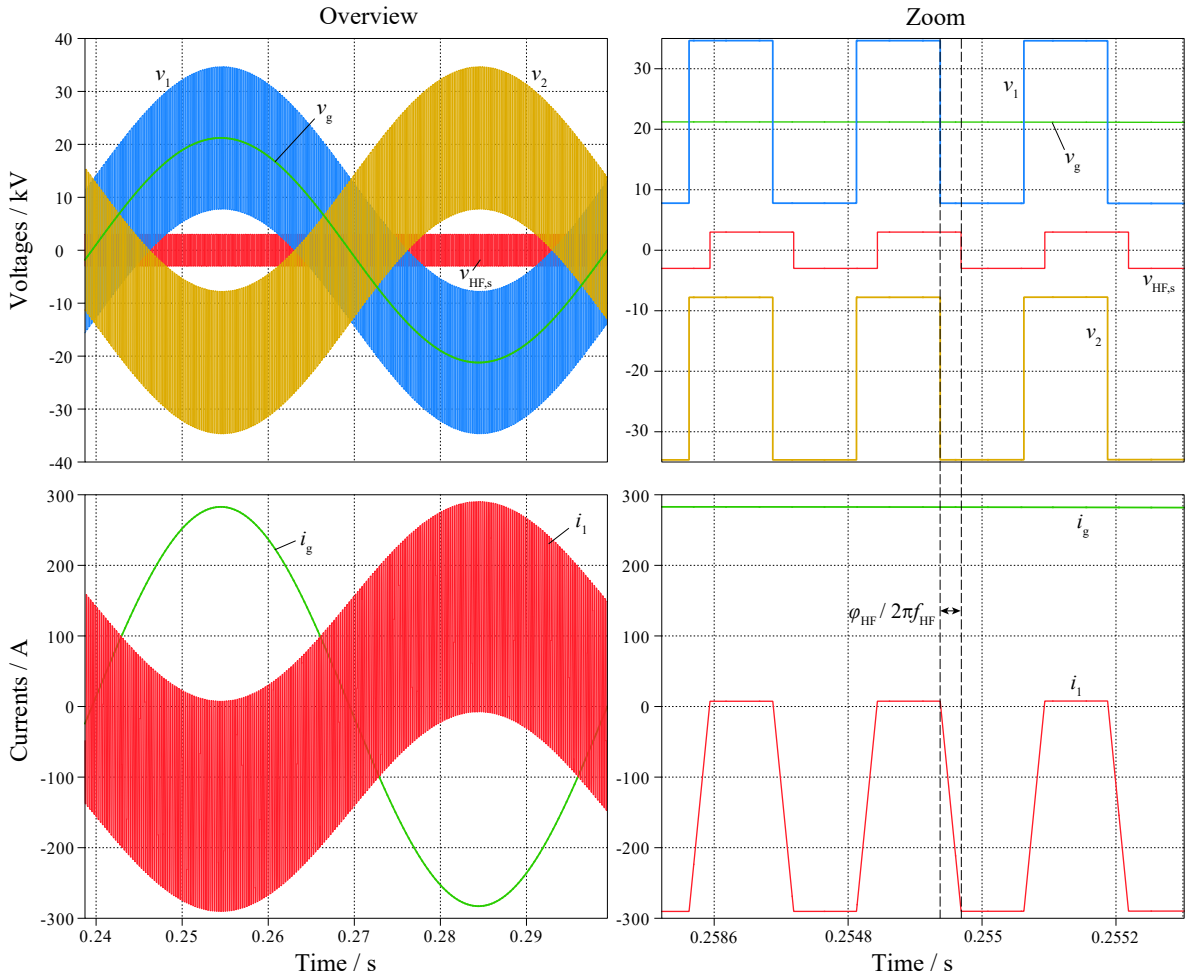

Fig. 2: Simulation results for the operation with $V_{dc} = 3\,\text{kV}$, $n = 4.5$, $f_{HF} = 4\,\text{kHz}$, $L_s = 2.8\,\text{mH}$ and $L_g = 10\,\text{mH}$. The phase shift φ_{HF} is $\pi/4$. Overview shown in the left, zoom-in shown in the right. The remaining system parameters are listed in Tab. I.

that the arm current i_1 has a zero crossing in each switching period throughout the complete grid period, such that ZVS is always achieved. This confirms the considerations in (7). Moreover, the HF current amplitudes also match with the equations presented before.

3 Comparison with existing PETT concepts

In the following, a comparison of the presented PETT concept with the concepts proposed in [3, 4] as depicted in Fig. 4 and [8] as depicted in Fig. 3 is conducted. The equations for the most important system parameters regarding cost and efficiency are derived and presented in Tab. II. Finally, a comparison is conducted for an exemplary parameter set as given in Tab. I.

3.1 Derivations for Concept proposed in [8]

The MMC arm voltage is

$$v_1(t) = V_g/2 \cdot \sin(\omega_g t) - n \cdot V_{dc}/2 \cdot \text{rect}(f_{HF} \cdot t). \tag{15}$$

Therefore the maximum MMC arm voltage results in $(V_g + V_{dc})/2$. The MMC arm current is composed of half the grid current and half the MFT current:

$$i_1(t) = i_g(t)/2 + i_{hf,s}(t)/2n \tag{16}$$

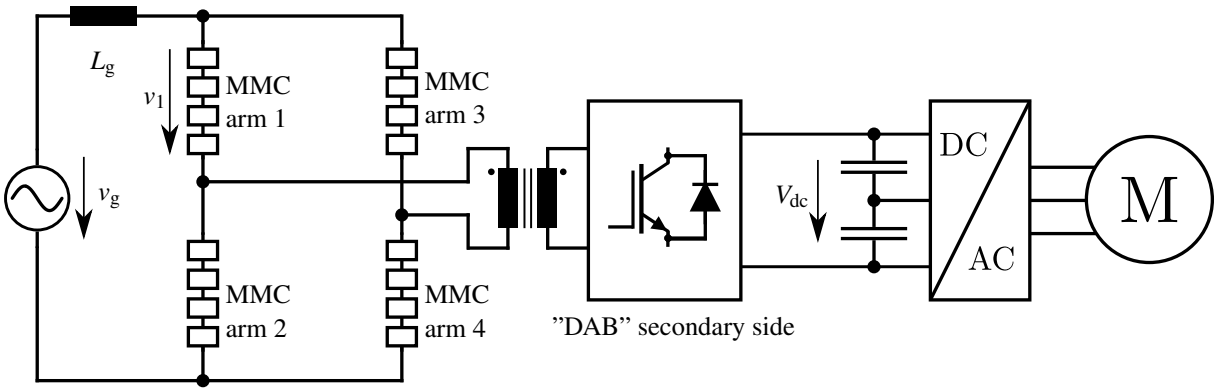

Fig. 3: MMC based PETT topology proposed in [8].

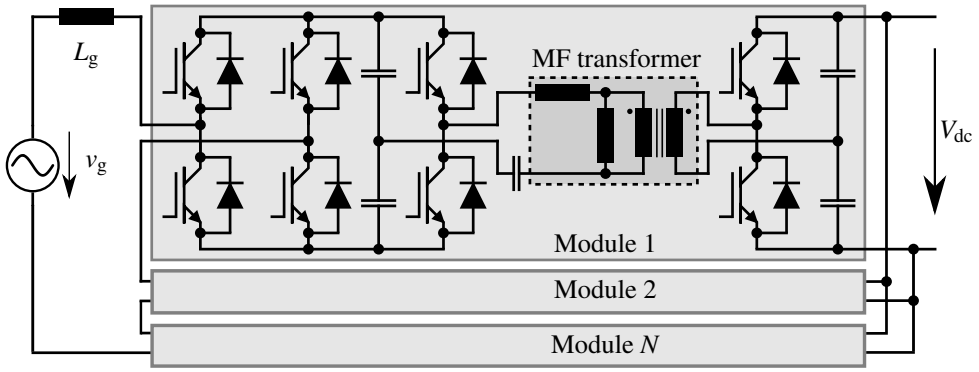

Fig. 4: MMC based PETT topology proposed in [3, 4].

Similarly, as explained for the PETT topology proposed in this paper (cf. (6)), the maximum arm current results in $I = {}^{P}/_{V_g} + {}^{2P}/_{3nV_{dc}}$.

The required number of modules, switches and the required semiconductor power are simple to calculate from here. Derivations are omitted for space reasons. The formulas are given in Tab. II.

To achieve a zero crossing of the current in all arms and therefore ZVS, the amplitude of the HF part of the current must be greater than the grid current part in the MMC arms. Because the arm currents are half of the transformer HF current and half of the grid current, the same equations as for the topology proposed in this paper hold for the transformer turns ratio n_{ZVS}. Note that this is not mentioned in [8].

Concerning the required energy storage in the module capacitors, similar considerations as for the topology proposed in this paper can be applied: Since the power from the grid and to the MFT is shared equally among the four individual MMC arms, e_{arm} and its peak-to-peak value Δe_{arm} compile to

$$e_{arm} = \int_0^t P_{LF}(t) - P_{HF} dt = \int_0^t \frac{P}{2}\sin^2(\omega_g t) - \frac{P}{4} dt = -\frac{P}{8\omega_g} \quad \rightarrow \quad \Delta e_{arm} = \frac{P}{4\omega_g}. \tag{17}$$

Therefore, the total required average energy storage is the same as for the topology proposed in this paper:

$$C \geq \frac{P}{8N \cdot \omega_g \cdot V_m \cdot \Delta v_m} \quad \rightarrow \quad E_{cap} = 2 \cdot N \cdot C \cdot V_m^2 = \frac{V_m \cdot P}{4 \cdot \omega_g \cdot \Delta v_m}. \tag{18}$$

3.2 Derivations for Concept proposed in [3, 4]

With the concept proposed in [3, 4], the MMC arm voltage is equal to the grid voltage $V_g \cdot \sin(\omega_g t)$, such that the maximum arm voltage is V_g. Furthermore, the arm current is also equal to the grid current, such that the maximum arm current is $I_g = 2P/V_g$.

Table II: Comparison of basic PETT concepts

Parameter	This paper	[8]	[3, 4]
MMC arm max. voltage	$V_\mathrm{g}+n\cdot V_\mathrm{dc}$	$(V_\mathrm{g}+n\cdot V_\mathrm{dc})/2$	V_g
MMC arm max. current I	$P/V_\mathrm{g}+4P/3nV_\mathrm{dc}$	$P/V_\mathrm{g}+4P/3nV_\mathrm{dc}$	$2P/V_\mathrm{g}$
Min. number of modules N_tot	$2\cdot\lceil(V_\mathrm{g}+n\cdot V_\mathrm{dc})/V_\mathrm{m}\rceil$	$4\cdot\lceil(V_\mathrm{g}+n\cdot V_\mathrm{dc})/2V_\mathrm{m}\rceil$	$\lceil V_\mathrm{g}/V_\mathrm{m}\rceil$
Number of switches	$4N_\mathrm{tot}+4$	$4N_\mathrm{tot}+4$	$N_\mathrm{tot}\cdot(4+2+2)$
Min. semiconductor power	$4N_\mathrm{tot}\cdot I\cdot V_\mathrm{m}+4\cdot 4P/3$	$4N_\mathrm{tot}\cdot I\cdot V_\mathrm{m}+4\cdot 4P/3$	$4N_\mathrm{tot}\cdot I\cdot V_\mathrm{m}+4\pi\cdot P$
Energy storage	$(V_\mathrm{m}\cdot P)/(4\cdot\omega_\mathrm{g}\cdot\Delta v)$	$(V_\mathrm{m}\cdot P)/(4\cdot\omega_\mathrm{g}\cdot\Delta v)$	$(V_\mathrm{m}\cdot P)/(4\cdot\omega_\mathrm{g}\cdot\Delta v)$
Number of MFTs	1	1	N_tot
Volume MFTs	$\propto P^{3/8}$	$\propto P^{3/8}$	$\propto N_\mathrm{tot}\cdot(P/N_\mathrm{tot})^{3/8}$

The minimum required number of modules $N=\lceil V_\mathrm{g}/V_\mathrm{m}\rceil$ with the module voltage V_m also defines the minimum number of switches because there are 6 switches required for each module.

Because full-bridge modules with four switches are required, the installed semiconductor power for the MMC part is given by $4N\cdot I_\mathrm{g}\cdot V_\mathrm{m}$. For the half bride LLC resonant part, the current amplitude is given by $\pi/V_{dc}\cdot P/N$ when neglecting the magnetizing current and assuming an operation at resonance frequency (sinusoidal current, rectangular voltage). Therefore, the installed semiconductor power for the LLC resonant part of the PETT is $4\pi\cdot P$ because there are 4 switches per module that have to transfer the power P/N.

The required energy storage in the module capacitors can be derived on the same basis as shown for the other two topologies. Following similar considerations as in the previous section, the capacitive energy storage is the same as for the other two topologies.

3.3 Medium Frequency Transformer Scaling Laws

The scaling laws for MFTs [18] regarding a constant efficiency, the achievable apparent power of a transformer S_trafo per volume V_trafo (power density) is

$$\frac{S_\mathrm{trafo}}{V_\mathrm{trafo}}\propto x^{\frac{\beta}{\beta-2}} \tag{19}$$

with its linear dimension x and the Steinmetz parameter $\beta\in[2,3]$ for typical MFT core materials [18]. With $\beta=2.5$, the power density scales with x^5, such that

$$V_\mathrm{trafo}\propto\frac{S_\mathrm{trafo}}{x^5}=\frac{S_\mathrm{trafo}}{V_\mathrm{trafo}^{5/3}}\quad\Rightarrow\quad V_\mathrm{trafo}\propto S_\mathrm{trafo}^{3/8}, \tag{20}$$

because $V_\mathrm{trafo}=x^3$.
Considering the thermal limitation of a transformer design and therefore assuming a constant temperature rise, the achievable apparent power of a transformer S_trafo per volume V_trafo (power density) is

$$\frac{S_\mathrm{trafo}}{V_\mathrm{trafo}}\propto x^{-\frac{1}{\beta}}=x^{-\frac{1}{2.5}}. \tag{21}$$

Concerning the achievable volume this results in

$$\frac{S_\mathrm{trafo}}{V_\mathrm{trafo}}\propto(V_\mathrm{trafo}^{\frac{1}{3}})^{-\frac{1}{2.5}}=V_\mathrm{trafo}^{-\frac{2}{15}}\quad\Rightarrow\quad V_\mathrm{trafo}\propto S_\mathrm{trafo}^{15/13}, \tag{22}$$

because $x=V_\mathrm{trafo}^{1/3}$.

3.4 Evaluation with Exemplary Parameter Set

In Fig. 5, the minimum number of modules, the number of switches, and the installed semiconductor power (operating voltage times maximum switch current) and the transformer volume ratios for the

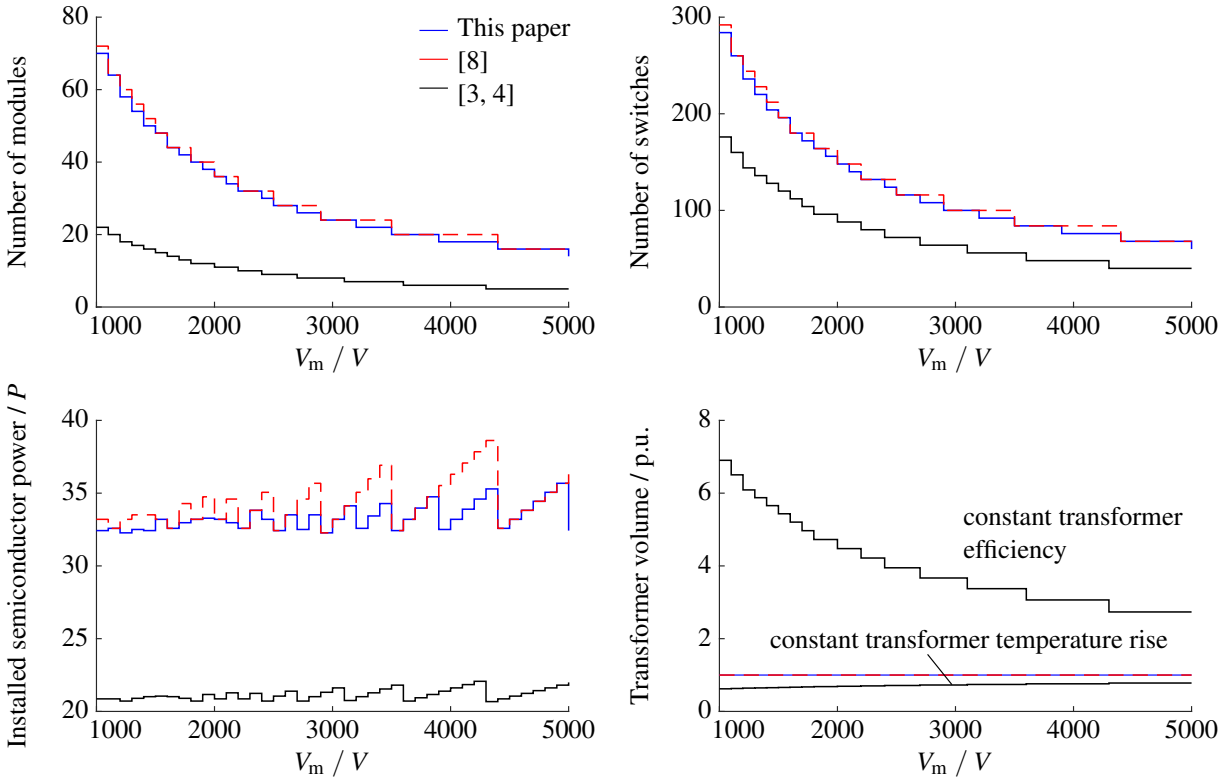

Fig. 5: Comparison of the implementation effort for the proposed concept, as well as the concepts presented in [8] and [3, 4] for a varying module voltage V_m. System parameters are given in Table I. For the concepts proposed in this paper and in [8], the transformer turns ratio n is set to n_{ZVS} (cf. (7)). Note that with the concept from [3, 4], the turns ratio is defined by the ratio between the module voltage and the secondary voltage amplitude V_{dc}. The transformer volume is given as a relation between the many small transformers required with the concept presented in [3, 4] and the single big transformer required for the concept presented in this paper or in [8] (set to 1 p.u.). Here, it is distinguished between the minimum achievable volume given a constant temperature rise and the necessary volume to achieve a constant efficiency.

considered concepts are compared for different module voltages. The parameters used for the comparison are summarized in Tab. I.

One can see, that regarding the number of modules as well as the required to be installed semiconductor power, the concept proposed in [3, 4] is always better than the concepts proposed in this paper and in [8].

The big drawback of the concept presented in [3, 4] is the fact that it needs an MFT in each and every module, such that the implementation effort per module is much higher than for the other concepts. Both MFT scaling laws presented in the previous section are considered in Fig. 5 to compare the transformer volume resulting from the different PETT concepts. Conceptually, if the same transformer efficiency should be achieved, the high number of required MFTs for the concept presented in [3, 4], results in a considerably higher total volume of the transformers of the PETT compared to the concept presented in this paper or [8]. If the efficiency is not first priority and maximum power density should be achieved, the high number of employed MFTs of [3, 4], results in a lower total volume of the transformers of the PETT compared to the concept presented in this paper or [8]. This is because many small transformers simplify the cooling compared to one single big transformer.
However, also an isolation voltage of at least the grid voltage also needs to be provided by all transformers, which is not represented by the scaling laws (20) and (22). Therefore, it would additionally increase the total volume of the many small transformers required with the concept of [3, 4].

When comparing the proposed concept and the one proposed in [8], the main parameters are very similar. This is especially true for the expressions as given in Tab. II. However, one needs to consider, that the

number of modules per MMC arm needs to be an integer number, such that four arms can lead to a higher total number of modules in the end. Therefore, the number of modules, the number of switches, as well as the installed semiconductor power with the proposed concept is always lower or equal to [8]. A drawback of the concept proposed in this paper is that the grid current needs to flow though the primary windings of the transformer. However, because of its very low frequency, the related skin and proximity losses are typically negligible and only the DC resistance of the primary windings is of relevance for the related transformer losses.

4 Conclusion

In this paper, a novel MMC based power electronic traction transformer concept is proposed. It can be implemented with only two standard MMC arms using full-bridge modules. In comparison to a similar concept existing in literature, it uses less MMC arms resulting in a lower control and modulation effort. Moreover, the total number of MMC modules can be lower for the same module voltage, such that the installed semiconductor power can be reduced. Other concepts from literature require multiple medium frequency transformers. This is avoided by the proposed concept, at the cost of a higher number of modules and increased installed semiconductor power. However, the proposed concept allows zero voltage switching for all employed switches.

References

[1] S. Farnesi, M. Marchesoni, M. Passalacqua, and L. Vaccaro, "Solid-state transformers in locomotives fed through AC lines: A review and future developments," *Energies*, vol. 12, no. 24, 2019.

[2] T. Guillod and J. W. Kolar, "Medium-frequency transformer scaling laws: Derivation, verif ication, and critical analysis," *CPSS Trans. on Power Electron. and Appl.*, vol. 5, no. 1, 2020.

[3] D. Dujic, C. Zhao, A. Mester, J. K. Steinke, M. Weiss, S. Lewdeni-Schmid, T. Chaudhuri, and P. Stefanutti, "Power electronic traction transformer-low voltage prototype," *IEEE Trans. on Power Electron.*, vol. 28, no. 12, 2013.

[4] C. Zhao, D. Dujic, A. Mester, J. K. Steinke, M. Weiss, S. Lewdeni-Schmid, T. Chaudhuri, and P. Stefanutti, "Power electronic traction transformer—medium voltage prototype," *IEEE Trans. on Ind. Electron.*, vol. 61, no. 7, 2014.

[5] J. E. Huber and J. W. Kolar, "Optimum number of cascaded cells for high-power medium-voltage AC–DC converters," *IEEE Journal of Emerging and Sel. Topics in Power Electron.*, vol. 5, no. 1, 2017.

[6] J. E. Huber, "Conceptualization and multi-objective analysis of multi-cell solid-state transformers," PhD Thesis, ETH Zürich, 2016.

[7] P. Simiyu and I. E. Davidson, "MVDC railway traction power systems, state-of-the art, opportunities, and challenges," *Energies*, vol. 14, no. 14, 2021.

[8] M. Glinka and R. Marquardt, "A new AC/AC multilevel converter family," *IEEE Trans. on Power Electron.*, vol. 52, no. 3, 2005.

[9] R. DeDoncker, D. Divan, and M. Kheraluwala, "A three-phase soft-switched high-power-density DC/DC converter for high-power applications," *IEEE Trans. on Ind. Appl.*, vol. 27, no. 1, 1991.

[10] M. Kheraluwala, R. Gascoigne, D. Divan, and E. Baumann, "Performance characterization of a high-power dual active bridge DC-to-DC converter," *IEEE Trans. on Ind. Appl.*, vol. 28, no. 6, 1992.

[11] F. Krismer and J. W. Kolar, "Closed form solution for minimum conduction loss modulation of DAB converters," *IEEE Trans. on Power Electron.*, vol. 27, no. 1, 2012.

[12] M. Stojadinovic, E. Kalkounis, F. Jauch, and J. Biela, "Generalized PWM generator with transformer flux balancing for dual active bridge converter," in *18th Eur. Conf. on Power Electron. and Appl. (EPE, ECCE Europe)*, 2017.

[13] M. Kasper, R. Burkat, F. Deboy, and J. Kolar, "ZVS of power MOSFETs revisited," *IEEE Trans. on Power Electron.*, 2016.

[14] K. Ilves, S. Norrga, L. Harnefors, and H.-P. Nee, "On Energy Storage Requirements in Modular Multilevel Converters," *IEEE Trans. on Power Electron.*, vol. 29, no. 1, 2014.

[15] S. Fuchs, M. Jeong, and J. Biela, "Reducing the energy storage requirements of modular multilevel converters with optimal capacitor voltage trajectory shaping," in *22nd Eur. Conf. on Power Electron. and Appl. (EPE, ECCE Europe)*, 2020.

[16] S. Fuchs, "MMCs Made Compact and Fast - Towards Modular Multilevel Converters with Minimized Module Capacitance and Fast Transient Operation Utilizing Advanced Control Methods," PhD Thesis, ETH Zürich, 2022.

[17] H. Bärnklau, A. Gensior, and S. Bernet, "Derivation of an equivalent submodule per arm for modular multilevel converters," in *15th Int. Power Electron. and Motion Control Conf. (EPE/PEMC)*, 2012.

[18] C. R. Sullivan, B. A. Reese, A. L. F. Stein, and P. A. Kyaw, "On size and magnetics: Why small efficient power inductors are rare," in *Int. Symposium on 3D Power Electron. Integration and Manufacturing*, 2016.